Unstable dynamics of solitary traveling waves in a lattice with long-range interactions

Henry Duran[1], Haitao Xu[2], Panayotis G. Kevrekidis[3], and Anna Vainchtein[1]

[1]Department of Mathematics, University of Pittsburgh, Pittsburgh, Pennsylvania 15260, USA
[2]Center for Mathematical Science, Huazhong University of Science and Technology, Wuhan, Hubei 430074, People's Republic of China
[3]Department of Mathematics and Statistics, University of Massachusetts, Amherst, MA 01003-9305, USA

August 30, 2021

Abstract

In this work we revisit the existence, stability and dynamics of traveling solitary waves in the context of lattice dynamical systems. We consider a nonlinear lattice of an α-Fermi-Pasta-Ulam type with the additional feature of all-to-all harmonic long-range interactions whose strength decays exponentially with distance. The competition between the nonlinear nearest-neighbor terms and the longer-range linear terms yields two parameter regimes where the dependence of the energy H of the traveling waves on their velocity c is non-monotonic and multivalued, respectively. We examine both cases, and identify the exact (up to a prescribed numerical tolerance) traveling waves. To investigate the stability of the obtained solutions, we compute their Floquet multipliers, thinking of the traveling wave problem as a periodic one modulo shifts. We show that in the general case when the relationship between H and c is not necessarily single-valued, a stability threshold corresponds to $H'(s) = 0$, where s is the parameter along the energy-velocity curve. Perturbing the unstable solutions along the corresponding eigenvectors, we identify two different scenarios of the dynamics of their transition to stable branches. In the first case, the perturbed wave slows down after expelling a dispersive wave. The second scenario involves an increase in the velocity of the perturbed wave accompanied by the formation of a slower small-amplitude traveling solitary wave.

Keywords: lattice dynamics, long-range interactions, traveling solitary wave, Floquet spectrum, instability, energy-based criterion

1 Introduction

Since the groundbreaking work [1, 2] on nonlinear Fermi-Pasta-Ulam (FPU) lattices, among the principal objects of investigation have been the solitary traveling waves (STWs) that emerge therein and their connection to soliton solutions of the Korteweg-de Vries (KdV) equation. Consequently, many studies have been devoted to understanding the properties of these waves in discrete systems, including experimental investigations in electrical networks [3, 4], granular materials [5–7], and more recently in mechanical metamaterials [8, 9] and lipid monolayers [10]. Significant theoretical developments include the discovery of the integrable Toda lattice and the study of its STWs [11], existence proofs for non-integrable systems [12–15] and rigorous investigations of the low-energy [16–22] and high-energy [23–25] limits. In addition to STWs, many other types of nonlinear phenomena in discrete systems have been investigated, including recent studies of modulational instabilities [26] and dispersive waves [27] in repulsive lattices.

Despite all this progress, stability of lattice STWs remains an issue that is far from being fully understood, with rigorous results only known for some special cases such as the integrable Toda lattice [28, 29], near-integrable sonic limit [16–19] and the hard-sphere high-energy limit [25]. A sufficient condition for change in the spectral stability of a STW was established in [18] for the FPU problem. In the recent work [30, 31] this result was extended to a general class of Hamiltonian systems and connected to stability criteria in the realm of discrete breathers [32]. This energy-based criterion involves the monotonicity of the Hamiltonian H as a function of the wave's velocity c. The corresponding criterion for breathers, time-periodic localized solutions, concerns the monotonicity of H with respect to the frequency ω of the breather. The intimate connection between the criteria stems from the fact that traveling waves are periodic modulo lattice shifts, resulting in the direct proportionality of ω and c. The relevant stability criterion states that as c is varied, passing through a critical point of $H(c)$ is sufficient (but not necessary) for a change in stability. As shown in [30, 31], a pair of eigenvalues associated with the STW collides at zero at the critical velocity value and reemerges on the real axis when the wave becomes unstable.

The combination of this criterion and the fact that STWs in the FPU problem are stable near the sonic limit, where $H'(c) > 0$ [19] suggests that waves become unstable when $H'(c) < 0$. We note that the marginal case $H'(c) = 0$ needs to be treated separately and is outside the scope of the present work. Interestingly, in most known cases $H(c)$ is a monotonically increasing function and numerical (or, in the case of Toda lattice, analytical [28,29]) results indicate stability of all STWs. Examples of lattices with nonmonotone $H(c)$ include systems with piecewise quadratic interaction potentials [33–36] and their smooth approximations [31]. Another remarkable example was revealed in a series of papers [37–40] that investigated a lattice with nonlinear nearest-neighbor interactions and harmonic Kac-Baker [41, 42] longer-range interactions. Accounting for such effects is important in modeling real physical systems, such as chains of uncharged molecular units with non-negligible dipole-dipole interactions. The exponential decay of the Kac-Baker interactions has been used to obtain closed-form expressions for various thermodynamic quantities in Ising [41, 42], Potts [43] and Klein-Gordon [44] models. In [37–40], the authors showed that depending on the parameters of the long-range interactions and due to an interplay of two different length scales, $H(c)$ can be monotonically increasing, nonmonotone or fold on itself (Z-shaped), becoming multivalued in a certain velocity interval, where three STWs with the same velocity coexist [40]. Numerical simulations in [40] suggest stability of the low-energy and high-energy solutions where $H'(c) > 0$ and instability of the solutions with the intermediate energy values. For the nonmonotone single-valued case, this conjecture is supported by the stability analysis of the associated quasicontinuum model in [39] and linear stability analysis of the discrete system in [30,31] which reveals the above mentioned instability picture associated with real eigenvalues at the spectral analysis level.

In this work we revisit this problem and extend the analysis in [30,31] to the case when $H(c)$ is no longer single-valued. We show that the change of stability is now associated with the change of sign of $H'(s)$, where s is the parameter that c and H depend on. Representing STWs as periodic-modulo-shift orbits [18,30,31], we perform Floquet analysis in the parameter regime where $H(c)$ is Z-shaped and show that instability in this case is associated with $H'(s) < 0$. In the case of a nonmonotone single-valued $H(c)$ function this reduces to $H'(c) < 0$.

A related central scope of this work is to investigate in detail the dynamical consequences of instability in both of these regimes. We do this by perturbing the unstable waves along the eigenmode corresponding to a real Floquet multiplier associated with the instability and tracking the velocity and energy of the evolving wave. Our results show that depending on the sign of perturbation, there are two generic scenarios. In the first case, the wave slows down after expelling a dispersive shock wave. In the second scenario, the wave's velocity increases following the formation and expulsion of a small-amplitude STW. In both cases, the waves stabilize when their velocity reaches a value along the energy-velocity curve where $H'(c) > 0$.

The remainder of the paper is organized as follows. In Sec. 2 we formulate the problem and review prior results. In Sec. 3 we describe the numerical methods we used. Results for the single-valued nonmonotone $H(c)$ are presented in Sec. 4, while Sec. 5 is devoted to the multivalued case. Concluding remarks can be found in Sec. 6. A more technical stability analysis for multivalued $H(c)$ is presented in the Appendix.

2 Problem formulation and prior results

We consider Hamiltonian dynamics of a one-dimensional lattice with nonlinear nearest-neighbor interactions and all-to-all harmonic longer-range interactions, with moduli that decay exponentially with distance. The Hamiltonian of this system is given by

$$H = \sum_{n=-\infty}^{\infty} \left\{ \frac{1}{2}\dot{u}_n^2 + V(u_{n+1} - u_n) + \frac{1}{4} \sum_{m=-\infty}^{\infty} \Lambda(m)(u_n - u_{n+m})^2 \right\}, \tag{1}$$

where $u_n(t)$ denotes the displacement of nth particle at time t, $\dot{u}_n = u_n'(t)$, and $V(w) = w^2/2 - w^3/3$ is the potential governing the nonlinear nearest-neighbor interactions. The last term represents Kac-Baker interactions that have moduli $\Lambda(m) = J(e^{\alpha} - 1)e^{-\alpha|m|}(1 - \delta_{m,0})$. Here $J > 0$ measures the intensity of the longer-range interactions, and $\alpha > 0$ determines their inverse radius. In terms of strain (relative displacement) variable $w_n = u_{n+1} - u_n$, equations of motion are

$$\ddot{w}_n + 2V'(w_n) - V'(w_{n+1}) - V'(w_{n-1}) + \sum_{m=1}^{\infty} \Lambda(m)(2w_n - w_{n+m} - w_{n-m}) = 0. \tag{2}$$

The energy H and the total momentum

$$P = \sum_{n=-\infty}^{\infty} \dot{u}_n \tag{3}$$

of the system are conserved in time.

Previous work [30,31,37–40] on this model has focused on *solitary traveling wave* (STW) solutions of (2), which have the form

$$w_n(t) = \phi(\xi), \quad \xi = n - ct, \tag{4}$$

where c is the wave's velocity, and vanish at infinity. These solutions satisfy the advance-delay differential equation

$$c^2\phi''(\xi) + 2V'(\phi(\xi)) - V'(\phi(\xi+1)) - V'(\phi(\xi-1)) + \sum_{m=1}^{\infty} \Lambda(m)(2\phi(\xi) - \phi(\xi+m) - \phi(\xi-m)) = 0. \tag{5}$$

Numerical computations in [30, 31, 39, 40] suggest the existence of even ($\phi(-\xi) = \phi(\xi)$), compressive ($\phi(\xi) < 0$) solutions of this type with $c > c_{\mathrm{s}}$, where

$$c_{\mathrm{s}} = \sqrt{1 + J\frac{1 + e^{-\alpha}}{(1 - e^{-\alpha})^2}} \tag{6}$$

is the sound speed [40]. Due to the translational invariance of (5), these waves can be shifted arbitrarily along the ξ axis. Note also that the traveling wave solutions (4) are periodic modulo one lattice shift, $w_{n+1}(t + T) = w_n(t)$, with period $T = 1/c$, and thus can be viewed as fixed points of the map

$$\begin{bmatrix} \{w_{n+1}(T)\} \\ \{\dot{w}_{n+1}(T)\} \end{bmatrix} \to \begin{bmatrix} \{w_n(0)\} \\ \{\dot{w}_n(0)\} \end{bmatrix}. \tag{7}$$

In [39,40] the lattice equations (2) are approximated by a quasicontinuum model, which yields the traveling wave equation

$$(\partial_\xi^2 - s_+^2)(\partial_\xi^2 - s_-^2)\phi(\xi) = \frac{12}{c^2}(\partial_\xi^2 - \kappa^2)\phi^2(\xi), \tag{8}$$

where $\kappa = 2\sinh(\alpha/2)$ and

$$s_\pm^2 = \frac{1}{2}\left\{\kappa^2 + 12\frac{c^2-1}{c^2} \pm \sqrt{\left(\kappa^2 - 12\frac{c^2-1}{c^2}\right)^2 + 48\kappa^2\frac{c_s^2-1}{c^2}}\right\}. \tag{9}$$

Detailed analysis of the quasicontinuum approximation (8) in [39] (see also [38]) has shown that the interplay of short-range and long-range interactions in the problem gives rise to two competing velocity-dependent length scales $1/s_-$ and $1/s_+$, with $s_\pm$ given in (9). In a certain parameter regime, this scale competition leads to the existence of two branches of STWs, associated with low and high velocities, respectively, and the emergence of crest-like waves when the velocity reaches a critical value.

Numerical computations in [40] of solutions of (5) for the discrete problem further showed that the (α, J) plane can be subdivided into three regions, separated by the curves $J_1(\alpha)$ and $J_2(\alpha)$, where

$$J_1 \approx \begin{cases} 0.23\dfrac{\alpha^4}{\alpha_1^2 - \alpha^2}, & \alpha < \alpha_1 \\ \infty, & \alpha \geq \alpha_1, \end{cases} \qquad J_2 \approx \begin{cases} \dfrac{3\alpha^4}{8(\alpha_2^2 - \alpha^2)}, & \alpha < \alpha_2 \\ \infty, & \alpha \geq \alpha_2 \end{cases} \tag{10}$$

and $\alpha_1 = 0.25$, $\alpha_2 = 0.16$. These three regions are shown in Fig. 1. They consist of the M-region, where the energy H of the STW monotonically increases with its velocity c, the N-region, where the dependence is *nonmonotone*, with $H(c)$ initially increasing, then decreasing for a certain velocity interval and then increasing again, and lastly the Z-region, where the function $H(c)$ becomes *multi-valued* for some velocities ("Z-shaped"). The three different regimes were also captured in [37] using a collective-coordinate approach.

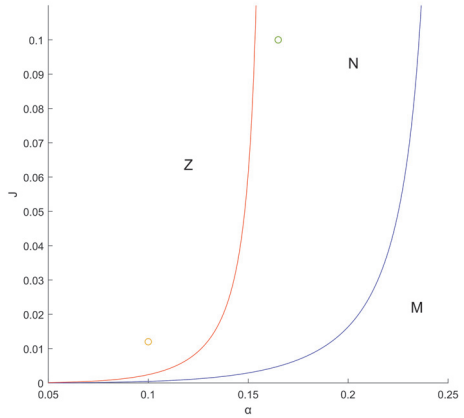

Figure 1: The M, Z and N-regions in the (α, J) plane together with the boundary curves $J_1(\alpha)$ (right) and $J_2(\alpha)$ (left) defined in (10). Circles mark the parameter values for the examples discussed in Sec. 4 and Sec. 5.

It has been conjectured in [40] that in the N and Z-regions the low-velocity and high-velocity solutions where $H'(c) > 0$ are stable, while waves along the intermediate branch are unstable. These assertions are supported by the stability analysis in [39] for the quasicontinuum model (8), where the stability threshold is linked to the change of monotonicity of the canonical momentum as the function of the velocity c of the wave, which appears to coincide with the corresponding change in

the monotonicity of $H(c)$. In [18] an analogous energy-based criterion, associating the change in the multiplicity of the zero eigenvalue for the linearized problem with the change of sign of $H'(c)$, was proved for the FPU problem without long-range interactions, and in [30,31] this result was extended to a general class of discrete systems with Hamiltonian H being a single-valued function of c. Moreover, explicit leading-order expressions for the pertinent pair of eigenvalues that meet at the origin at the stability threshold and emerge on the real axis at velocity values corresponding to the unstable waves were obtained in [30, 31]. For the problem at hand, this general result was illustrated in [30, 31] by considering STWs in the N-region and investigating linear stability in two different ways: the spectral analysis of the linear operator associated with the traveling wave equation (5) and the Floquet analysis of the linearization of the map (7). Both approaches corroborated the conjecture in [40] for the N-region. In particular, the waves corresponding to $H'(c) < 0$ are unstable.

In what follows we investigate in detail the consequences of this instability by perturbing the unstable STWs along the corresponding Floquet eigenvectors. To extend these results to the Z-region, where H is a multivalued function of c, we generalize the energy-based stability result in [30, 31] and show that in this case the instability threshold is associated with $H'(s)$ crossing zero, where s is a parameter that both H and c depend on (see the Appendix for the proof that the multiplicity of the zero eigenvalue increases at this threshold). We verify this result and the conjecture in [40] by conducting the Floquet analysis in the Z-region and investigate the corresponding unstable dynamics of STWs associated with $H'(s) < 0$.

3 Numerical methods

To compute the STWs in the N-region for given J and α, we employ the collocation method and continuation approach described in [30, 31] to generate a one-parameter family of STWs (parametrized by the velocity c) by numerically solving the traveling wave equation (5) for STW solutions starting at an initial velocity just above the sound speed (6) and using the near-sonic solution of the quasicontinuum equation (8) as an initial guess. These waves are computed on the finite interval $(-L/2, L/2]$ with mesh size $\Delta\xi$ at the collocation points $\xi_j = j\Delta\xi$, $j = -N/2 + 1, \dots N/2$, where N is even and $L = N\Delta\xi$. The fast Fourier transform is used to approximate the second-order derivative term in (5), while the advance and delay terms $\phi(\xi \pm m)$ are evaluated at the corresponding collocation points that are well defined on the chosen mesh. Following [31], we used $L = 800$ and $\Delta\xi = 0.1$ for a typical computation. The resulting nonlinear system is solved numerically for each velocity value using the Newton iteration method.

To compute the STWs in the Z-region, where the energy H is multivalued for some velocities, we combine the numerical procedure described above with the pseudo-arclength continuation method [45] to traverse the turning points in the energy-velocity curve. In this case the traveling wave solution and its velocity c depend on the arclength-like parameter s. In this parameter range, we used $L = 1200$ and $\Delta\xi = 0.1$.

To investigate linear stability of the computed waves, we use Floquet analysis. To this end, we trace the time evolution of a small perturbation $\epsilon y_n(t)$ of the periodic-modulo-shift traveling wave solution $\hat{w}_n(t) = \phi(n-ct)$, where we recall (4). This perturbation is introduced in (2) via $w_n(t) = \hat{w}_n(t) + \epsilon y_n(t)$. The resulting $O(\epsilon)$ equation reads

$$\ddot{y}_n + 2V''(\hat{w}_n)y_n - V''(\hat{w}_{n+1})y_{n+1} - V''(\hat{w}_{n-1})y_{n-1} + \sum_{m=1}^{\infty} \Lambda(m)(2y_n - y_{n+m} - y_{n-m}) = 0. \qquad (11)$$

Then, in the framework of Floquet analysis, the stability properties of periodic orbits are resolved by diagonalizing the monodromy matrix $\mathcal{F}$ (representation of the Floquet operator in finite systems),

which is defined as

$$\begin{bmatrix} \{y_{n+1}(T)\} \\ \{\dot{y}_{n+1}(T)\} \end{bmatrix} = \mathcal{F} \begin{bmatrix} \{y_n(0)\} \\ \{\dot{y}_n(0)\} \end{bmatrix}, \tag{12}$$

where we recall that $T = 1/c$. We remark that the Floquet operator can be equivalently constructed in terms of the perturbations of strain and momenta variables, which is consistent with the formulation considered in the Appendix. For the symplectic Hamiltonian systems we consider in this work, the linear stability of the solutions requires that the monodromy eigenvalues μ (also called Floquet multipliers) lie on the unit circle. The presence of a multiplier satisfying $|\mu| > 1$ indicates an instability.

The Floquet multipliers μ are related to the eigenvalues λ of the operator associated with the linearized problem via $\mu = e^{\lambda/c}$, so that the eigenvalue satisfying $\mathrm{Re}(\lambda) > 0$ corresponds to an instability. As we will show, the instability takes place when $H'(s) < 0$, where s is the parameter along the energy-velocity curve. In the case when $H(c)$ is single-valued, as in the N-region, this simplifies to $H'(c) < 0$ [30, 31]. To find the Floquet multipliers, we construct the monodromy matrix using the numerical solution of (11) with periodic boundary conditions.

To investigate the unstable dynamics, we perturb the wave along the unstable eigenmode, setting the initial conditions $w_n(0) = \phi(n-n_0)+\epsilon y_{n-n_0}$ and $\dot{w}_n(0) = -c\phi'(n-n_0)+\epsilon z_{n-n_0}$ for $|n-n_0| \le L/2$, and $w_n(0) = \dot{w}_n(0) = 0$ for $1 \le n < n_0 - L/2$ and $n_0 + L/2 < n \le N$, with the typical eigenmode profiles for y_n and z_n being depicted in Fig. 3 and ϵ measuring the strength of the applied perturbation. Here we recall that L is the length of the interval on which the traveling wave $\phi(\xi)$ is numerically computed, with (even) L chosen large enough for the wave to decay sufficiently at the end; typically, we set $L = 800$. The computed wave is shifted by n_0 and padded by zeros so that the initial condition defined at $n = 1, \ldots, N$ has compact support. Here n_0 and N are chosen so that the ensuing waveforms can propagate for a sufficiently long time without boundary effects. Typically, we set $n_0 = 701$ and $N = 4001$. The equations of motion (2) are then solved numerically with this initial condition and periodic boundary conditions to investigate the fate of the unstable solution.

Of particular interest is the velocity of the ensuing waveform as a function of time. Recall that an STW solution (shifted by n_0) has the form $w_n(t) = \phi(n - n_0 - ct)$, so that if t_1 and t_2 are such that $w_{n_1}(t_1) = w_{n_2}(t_2) = \phi(0)$, we have $c = (n_2 - n_1)/(t_2 - t_1)$. Here t_1 and t_2 correspond to the times when the minimum value of the STW reaches the corresponding particles n_1 and n_2. In the case of unstable dynamics, the wave is no longer steady, as its velocity and form change with time, but locally these changes are small. With this in mind, we determine the times t_i^* at which the minimum of the waveform reaches the particle with $n_i = n_0 + i\Delta n$, $i = 1, \ldots, K$, and approximate $c(t_i^*)$ by

$$c_i = \frac{\Delta n}{t_{i+1}^* - t_i^*}. \tag{13}$$

Here n_K is the particle number reached by the wave near the end of the simulation. To compute t_i^* more precisely, we use cubic spline interpolation of the numerical data. Experimentally, we found that setting $\Delta n = 5$ was optimal, since this value provided some averaging and yielded final velocities that were the same up to $O(10^{-5})$ as the computations with $\Delta n = 3$ and $\Delta n = 1$.

Other quantities of interest are the (local) energy and momentum of the evolving STW as functions of time. To find these, we consider sample times $\tau_i = i\Delta t$, where $\Delta t = 0.02$. At each time $t = \tau_i$, we determine the particle at which the strain reached its minimal value and compute the energy and momentum of a portion of the chain centered at this particle. The length of the portion, which is the same for each sample time τ_i, is chosen so that the main body of the wave was included in it, which we took to be when the strain was of $O(10^{-4})$ at the ends. Typically, including 125 particles is sufficient. Notice that while the total energy H and momentum P of the lattice remain conserved over the dynamical evolution (up to the relative error of $O(10^{-12})$ in the simulations), the localized energy and momentum portions associated with the wave may vary over time, especially in the scenario of the

dynamical evolution of a spectrally unstable wave. In that light, these diagnostics are quite suitable for detecting the potential transformations of STWs as a result of their instability.

4 Unstable dynamics in the N-region

We start by investigating the unstable dynamics of STWs in the N region. While multiple simulations in different regimes have been conducted, we present below only the results for $\alpha = 0.165$, $J = 0.1$ that are representative of the instability patterns observed in this parameter region. The corresponding H and maximal real Floquet multiplier μ as functions of c are shown in Fig. 2.

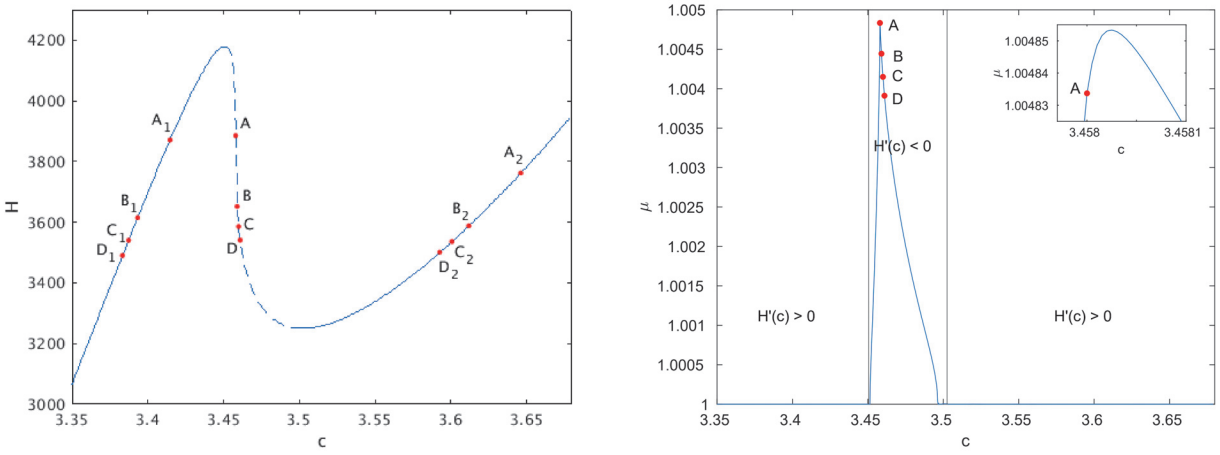

(a) (b)

Figure 2: (a) Energy H and (b) maximal real Floquet multiplier μ as functions of velocity c of the STWs at $(\alpha, J) = (0.165, 0.1)$. Unstable waves where $\mu > 1$ correspond to the decreasing dashed portion of the energy curve ($H'(c) < 0$). Points A, B, C, and D correspond to the velocities of the tested unstable waves, and points A_1, A_2, B_1, B_2, C_1, C_2, D_1, and D_2 mark the corresponding final velocities of the stable waves that the perturbed unstable STWs have evolved into, depending on the sign of the perturbation. Inset in (b) shows the enlarged view around the maximum.

Due to translational invariance, the system always has a pair of unit Floquet multipliers, which are the maximal real multipliers in the velocity intervals corresponding to increasing energy ($H'(c) > 0$). These velocity intervals apparently correspond to linearly stable STWs, although mild spurious oscillatory instabilities associated with complex Floquet multipliers slightly outside the unit circle may be present in this regime due to numerical artifacts that diminish as L is increased [31]. As the first stability threshold is crossed, a symmetric pair of imaginary eigenvalues λ collides at zero and reemerges on the real axis. Equivalently, a pair of multipliers sliding along the unit circle results in collision at the point $(1, 0)$ of the unit circle and reemerges on the real axis as a symmetric pair, with maximal real multiplier μ now exceeding unity (and the second multiplier of the pair now being inside the circle with a value of $1/\mu$), so that the corresponding STWs are unstable. The magnitude of μ increases, reaches a maximum value and then decreases again to unity when the second stability threshold is crossed. It should be noted that in the numerical computations $H'(c)$ is slightly below zero at the two stability thresholds. As discussed in [31], this is an artifact of the finite length L of the chain, and $H'(c)$ approaches zero at the threshold when L is increased.

To investigate the consequences of the instability associated with $\mu > 1$, we selected STWs with four different velocities inside the unstable interval and perturbed them along the corresponding eigenmodes, as described in Sec. 3. The simulations were run until a stable propagation pattern emerged. In all simulations, the perturbed unstable wave eventually evolves into a stable STW with lower energy

and either smaller or higher velocity, as shown in Fig. 2. We found that the size of the perturbation only affected the time it takes for the stable waveform to emerge but not the resulting wave itself. We also found that adding small random noise (of amplitude 10^{-4}) to the initial perturbation did not significantly affect the results; i.e., for a given unstable initial waveform, the dynamical evolution would apparently select a unique end state on the corresponding stable branches. A typical eigenmode used to initiate the instability is shown in Fig. 3. We note that each normalized eigenmode is determined up to plus or minus sign, so to change a wave from speeding up to slowing down or vice versa it suffices to reverse the sign of ϵ.

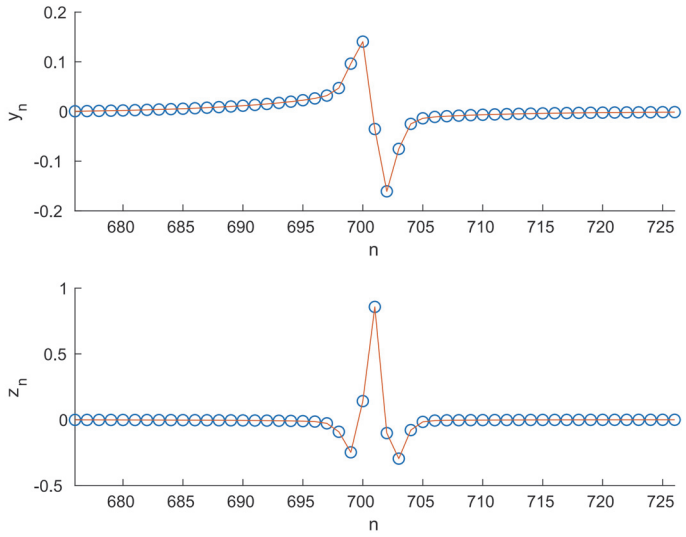

Figure 3: Eigenmode of an unstable STW with $c = 3.458$, $(\alpha, J) = (0.165, 0.1)$ corresponding to the Floquet multiplier $\mu = 1.0048$ that leads to the speeding up of the perturbed wave. Here y_n corresponds to strain and z_n to its time derivative. Reversing the sign of the perturbation results in slowing down of the perturbed wave. The red curve connecting the discrete points is included as a guide to the eye.

A representative example of velocity, energy and momentum evolution in the slow-down case is shown in Fig. 4. We observed that when the velocity of the perturbed unstable wave eventually decreases, the wave expels a small-amplitude dispersive shock wave, as can be seen in Fig. 5. As shown in Fig. 4(a), the velocity evolution in this case is nonmonotone: after initially decreasing, it briefly increases then decreases again to the final value. These velocity oscillations take place right around the time the dispersive wave formation becomes visible in the space-time plot shown in Fig. 5(a). Once this trailing dispersive wave detaches from the primary supersonic STW, the latter settles towards its final velocity. Note that while the energy of the wave decreases during this evolution, its momentum increases, with the total momentum of the system kept constant due to the negative contribution of the dispersive wave.

The dynamics is quite different when the velocity of the perturbed unstable wave increases (see Fig. 6). In this case, a small-amplitude STW, trailed by small-amplitude oscillations, forms behind the main waveform and eventually separates from it since it travels with smaller velocity; see Fig. 7. In this case the momentum of the primary wave decreases during the evolution due to the positive momentum of the slower wave.

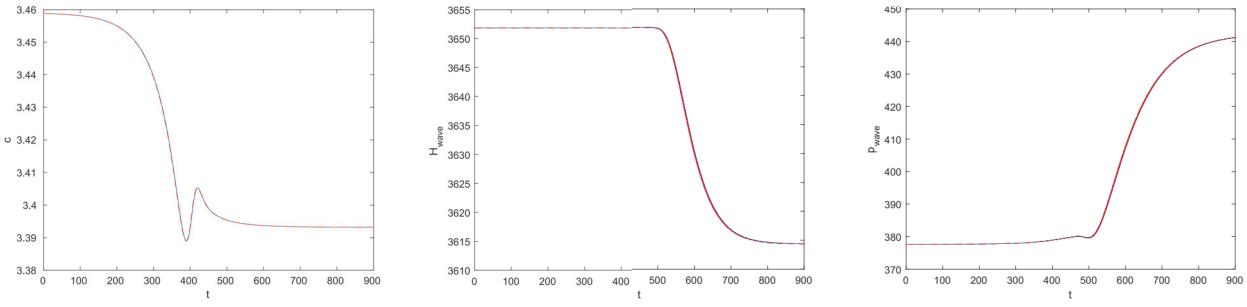

(a) (b) (c)

Figure 4: (a) Time evolution of the velocity of wave resulting from initial perturbation with $\epsilon = -0.25$ of the unstable STW with velocity 3.459 (point B in Fig. 2) at $(\alpha, J) = (0.165, 0.1)$. The velocity evolution is non-monotone: it initially decreases, then increases over a small time interval and then decreases again to the value 3.3932 (point B_1 in Fig. 2) towards the end of the simulation. (b) Time evolution of the energy of the STW. (c) Time evolution of the momentum of the STW. The red dashed lines show the evolution with small-amplitude random noise added to the initial perturbation, while the solid blue lines correspond to the simulations without the additional noise.

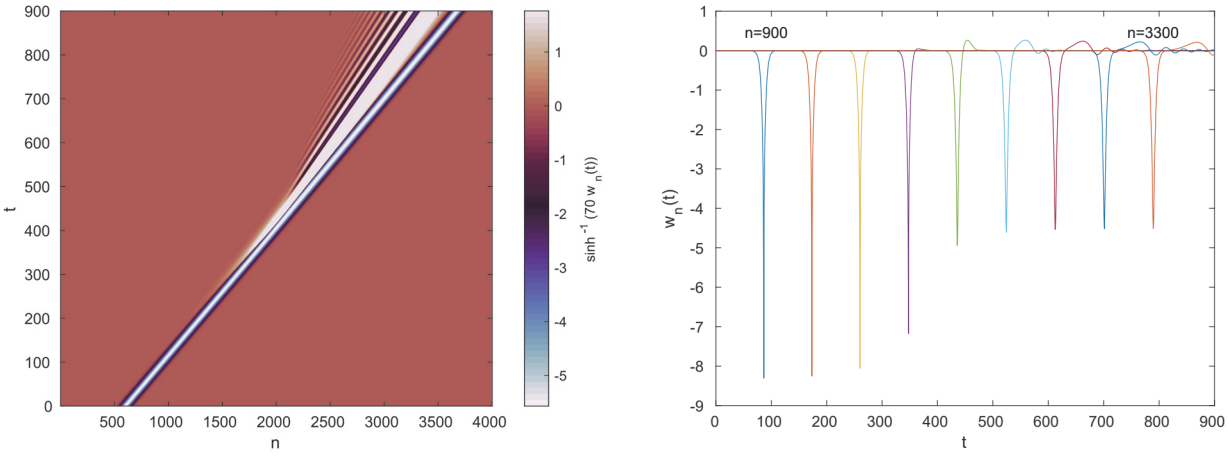

(a) (b)

Figure 5: (a) Space-time and (b) time evolution of $w_n(t)$ at fixed n during the transition from B to B_1 shown in Fig. 4. A primarily tensile dispersive shock wave is expelled by the main waveform as it slows down. Here $n_0 = 701$, and the selected values of n are spaced 300 units apart in (b). In (a) and other space-time plots shown below, we plot $\sinh^{-1}(70w_n)$ instead of w_n so that the structure of the expelled secondary waves is more visible.

5 Results for the Z-region

We now consider the Z-region. Recall that in this parameter region the function $H(c)$ becomes multivalued in a certain velocity interval. Using the pseudo-arclength algorithm, as described in Sec. 3, we computed such curves and analyzed the linear stability of the corresponding STWs for various parameter values in the region. Below we just describe the representative case $\alpha = 0.1$, $J = 0.012$. The energy-velocity plot for these parameter values is shown in Fig. 8(a). Along the curve $c = c(s)$ and $H = H(s)$, and each of these is a nonmonotone up-down-up function, so that both $H'(s)$ and $c'(s)$ change sign twice; i.e., $H(c)$ is triple-valued within a relevant interval of Fig. 8(a). However, the changes in monotonicity of $H(s)$ and $c(s)$ do not take place simultaneously, as can be seen in the insets of Fig. 8(a). Specifically, the first sign change for $H'(s)$, from positive to negative, occurs

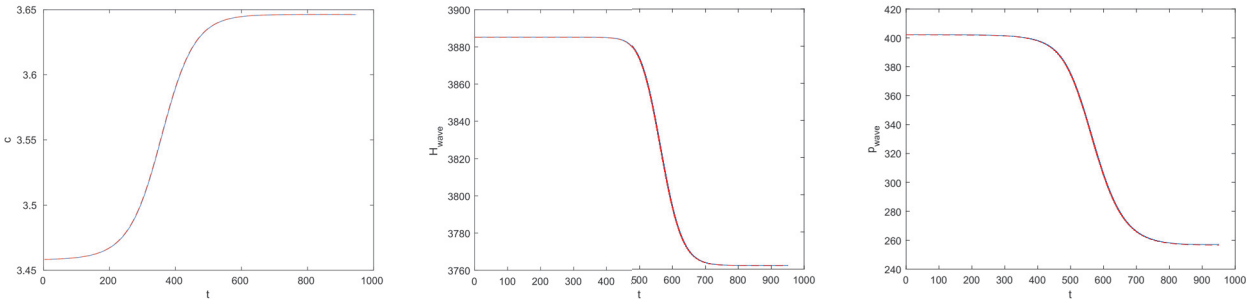

(a) (b) (c)

Figure 6: (a) Time evolution of the velocity of wave resulting from initial perturbation with $\epsilon = 0.25$ of the unstable STW with velocity 3.458 (point A in Fig. 2) at $(\alpha, J) = (0.165, 0.1)$. The velocity increases, approaching the value 3.6462 (point A_2 in Fig. 2) towards the end of the simulation. (b) Time evolution of the energy of the STW. (c) Time evolution of the momentum of the STW. The red dashed lines show the evolution with small-amplitude random noise added to the initial perturbation, while the solid blue lines correspond to the simulations without the additional noise.

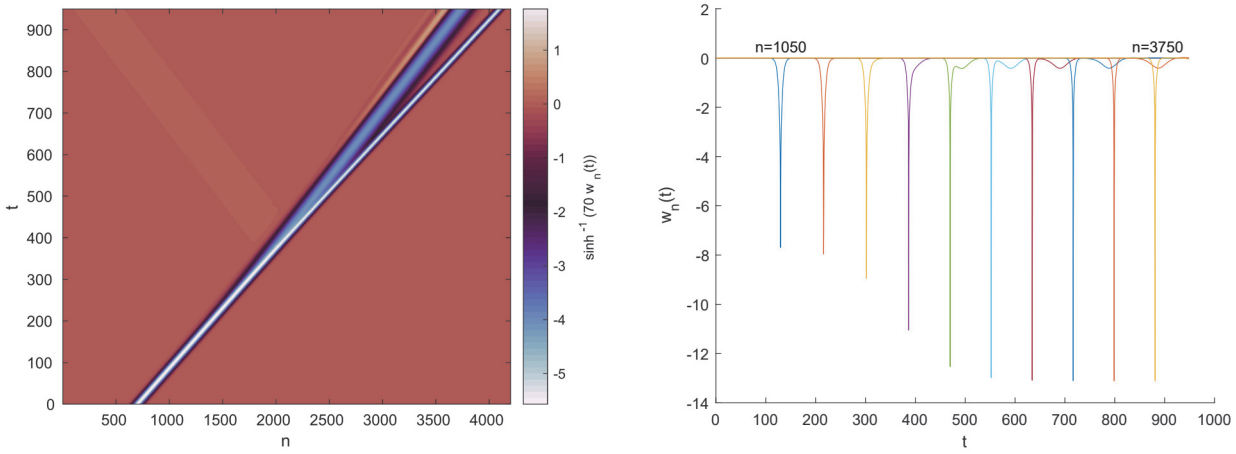

(a) (b)

Figure 7: (a) Space-time and (b) time evolution of $w_n(t)$ at fixed n during the transition from A to A_2 shown in Fig. 6. A compressive small-amplitude STW, trailed by small amplitude oscillations, forms behind the main nonlinear waveform and eventually separates from it as the main wave increases its velocity. Here $n_0 = 701$, and the selected values of n are spaced 300 units apart in (b).

slightly before $c(s)$ starts decreasing, and $c'(s)$ changes its sign back to positive prior to $H'(s)$. Thus we have $c'(s) > 0$ at both values of s where $H'(s)$ crosses zero.

As discussed in the Appendix, each threshold value of s where $H'(s) = 0$ corresponds to an increase in multiplicity of the zero eigenvalue of the operator associated with the linearized problem, which suggests a change in stability. The Hamiltonian nature of the problem implies that at the threshold value two symmetric imaginary eigenvalues meet at the origin and emerge on the real axis as $\pm\lambda$, $\lambda > 0$, as the wave becomes unstable, so that a real Floquet multiplier $\mu = \exp(\lambda/c) > 1$ appears in the unstable regime. To verify this for our numerically computed STWs, we plot in Fig. 8(b) the maximal real Floquet multiplier μ as the function of s for the obtained solutions. One can see that $\mu > 1$ in the interval of s that nearly coincides with the interval where $H'(s) < 0$ (similarly to the observations in the previous section, $H'(s)$ is slightly below zero at the threshold values due to the finite length of the computational domain, though this numerical artifact is not visible in Fig. 8(b)).

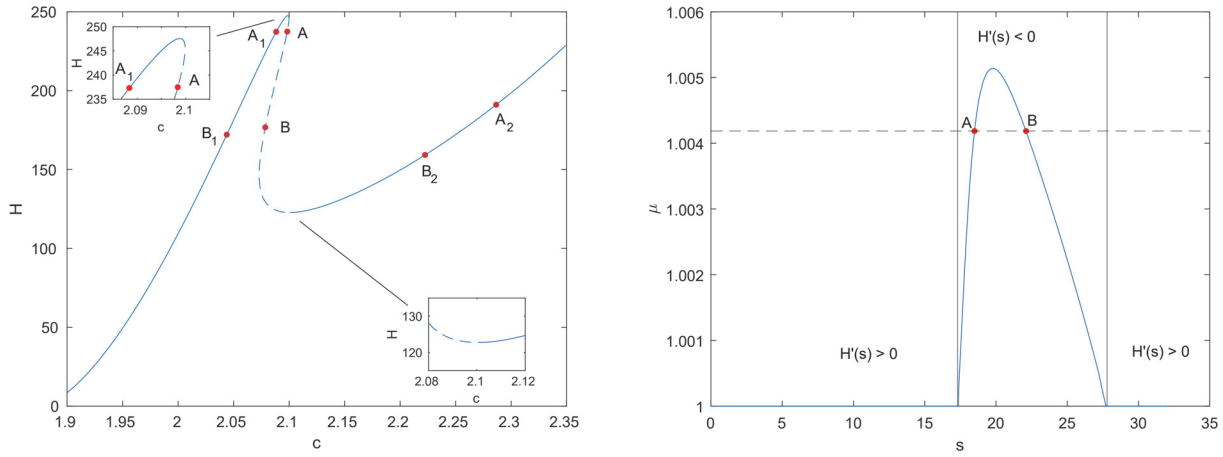

(a) (b)

Figure 8: (a) Energy H versus velocity c of STWs at $(\alpha, J) = (0.1, 0.012)$. Points A and B correspond to the energy and velocity of the tested waves, and points A_1, A_2, B_1, and B_2 mark the corresponding final velocities and energies of the stable waves the perturbed unstable STWs have evolved into. The dashed line corresponds to the portion of the curve where $H'(s) < 0$, and insets zoom in around the points where $H'(s) = 0$. (b) Maximal real Floquet multiplier μ as a function of the parameter s. The solid vertical lines indicate the values of s where $H'(s) = 0$. The dashed horizontal line marks the value $\mu = 1.0042$. In both figures, point A corresponds to the STW with velocity 2.0984 and point B corresponds to the STW with velocity 2.0785.

Thus, three STWs coexist for each c in the velocity interval where $c'(s) < 0$. Among these, the waves where $H'(s) < 0$ are unstable. This always includes the intermediate-energy wave, in agreement with the numerical observations in [40], but low-energy and high-energy waves also become unstable near the left and right ends of the velocity interval, respectively.

The splitting of the zero eigenvalue and transition to instability near the maximum and minimum of $H(s)$ are illustrated in Fig. 9. The plots show $\nu^2(s)$, where $\nu(s) = \lambda(s)/c(s)$ is a rescaled near-

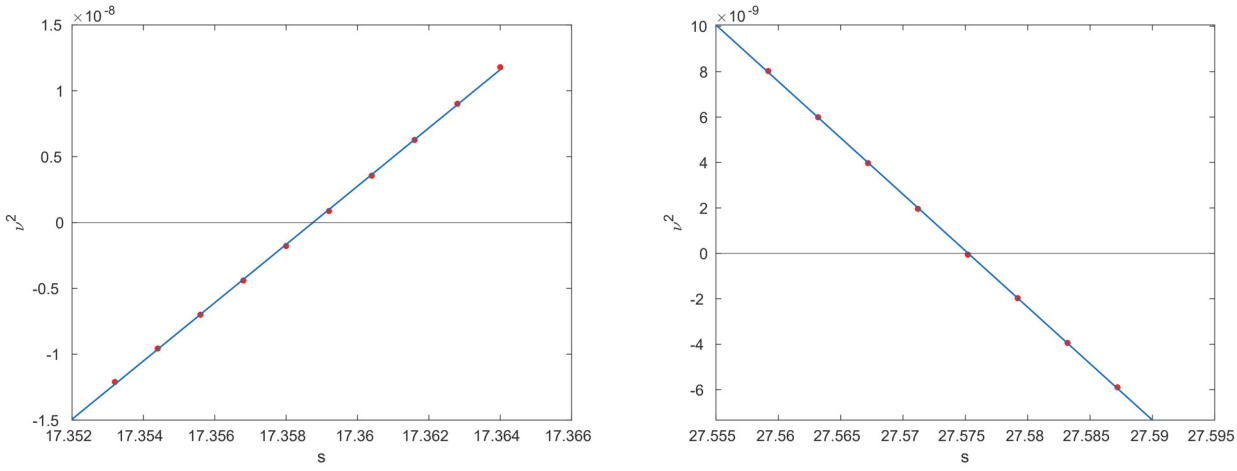

(a) (b)

Figure 9: Squared rescaled near-zero eigenvalues $\nu(s) = \lambda(s)/c(s) = \ln(\mu(s))$ near (a) the maximum and (b) the minimum of $H(s)$ at $(\alpha, J) = (0.1, 0.012)$. The straight lines show the best linear fit in each case. The black horizontal lines mark $\nu = 0$.

zero eigenvalue (note that $\nu = \ln(\mu)$, where μ is the corresponding Floquet multiplier near 1). As the stability threshold is crossed into the unstable region in each case, a symmetric pair of purely imaginary eigenvalues ($\nu^2 < 0$) becomes a symmetric pair of real eigenvalues ($\nu^2 > 0$). We note that $\nu^2 \sim s - s_0$ near each threshold s_0 is in agreement with the approximation derived in [30,31] (however, see the Appendix for the discussion of the effect of a weighted-space strain formulation that destroys the Hamiltonian structure of the problem on the multiplicity of the zero eigenvalue at the stability threshold).

We now examine the dynamical fate of unstable solutions. We consider two cases with velocities 2.0785 and 2.0984 that have the same Floquet multiplier $\mu = 1.0042$, which corresponds to eigenvalues $\lambda = 0.0087$ and 0.0088, respectively. Similar to the previously discussed cases for the N-region, the waves either slow down after expelling a dispersive wave or speed up after expelling a small-amplitude solitary wave, depending on the sign of the perturbation ϵ.

The slowing-down case for the unstable STW with velocity 2.0785 (point B in Fig. 8) is shown in Fig. 10 and Fig. 11. Note that the wave's velocity experiences a highly nonmonotone evolution in

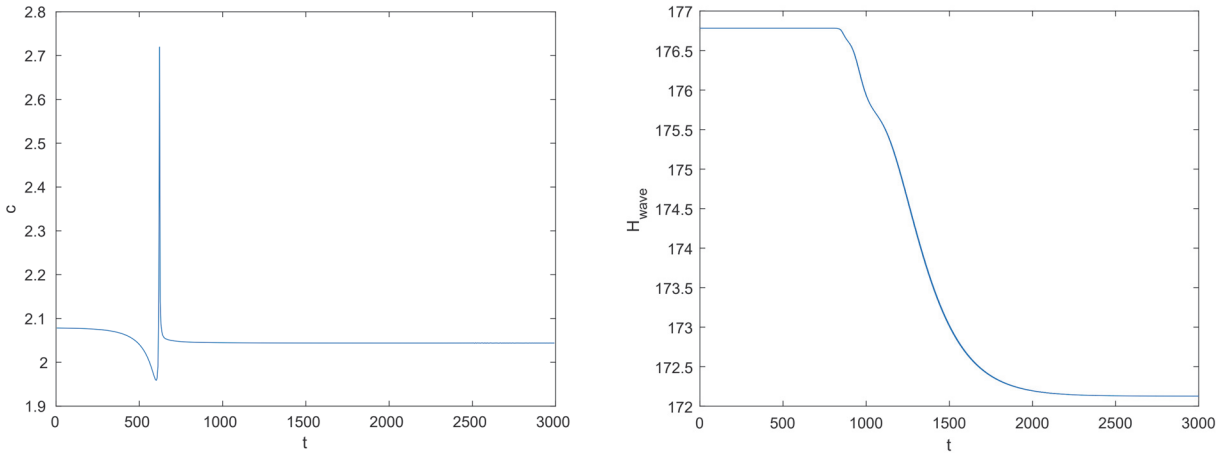

(a) (b)

Figure 10: (a) Time evolution of the velocity of wave resulting from initial perturbation with $\epsilon = -0.25$ of the unstable STW with velocity 2.0785 (point B in Fig. 8(a)) at $(\alpha, J) = (0.1, 0.012)$. The final velocity is 2.0439 (point B_1 in Fig. 8(a)). (b) Time evolution of the energy of the STW.

this case but eventually settles down to a lower value than the speed of the perturbed wave (point B_1 in Fig. 8(a)), as can be seen in Fig. 10(a). Fig. 12 zooms in the space-time plot of $w_n(t)$ in the time interval that includes times when the propagation velocity in Fig. 10(a) reaches its minimum and maximum. One can see that expulsion of the dispersive wave starts shortly after the velocity reaches its peak value.

When the sign of the perturbation is reversed, the wave speeds up after expelling a small-amplitude STW, and the ensuing dynamics is similar to the one shown in Fig. 6 and Fig. 7 for the N-region. Similar slowing-down and speeding-up scenarios are observed for simulations perturbing the unstable wave that corresponds to point A in Fig. 8(a).

6 Concluding remarks

In the present work we have revisited the existence, stability and dynamical features of lattice traveling waves in models where the competition between short-range nonlinear interactions and longer-range

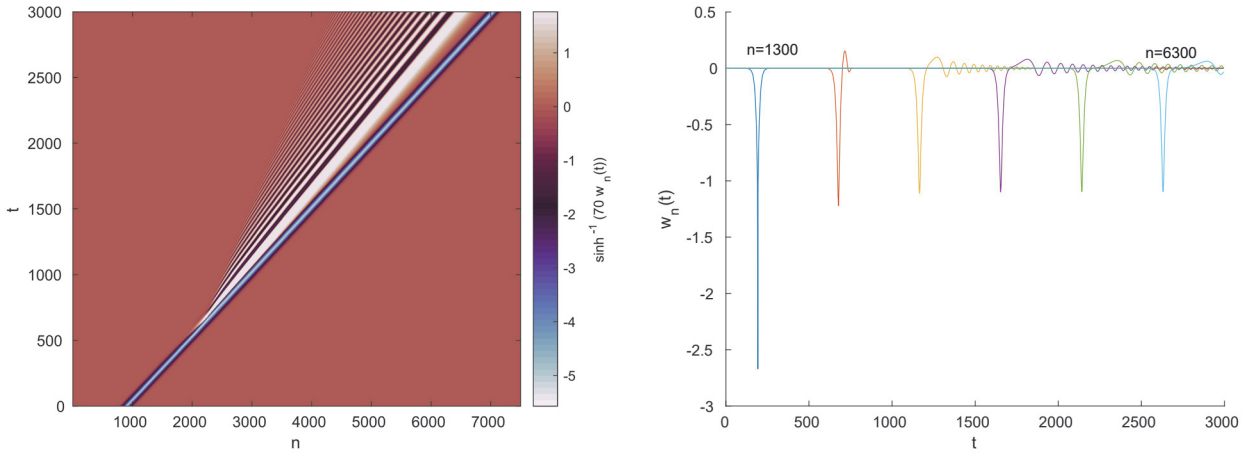

(a) (b)

Figure 11: (a) Space-time and (b) time evolution of $w_n(t)$ at fixed n during the transition from B to B_1 shown in Fig. 10. A dispersive shock wave is expelled by the main waveform as it slows down. Here $n_0 = 901$, and the selected values of n are spaced 1000 units apart in (b).

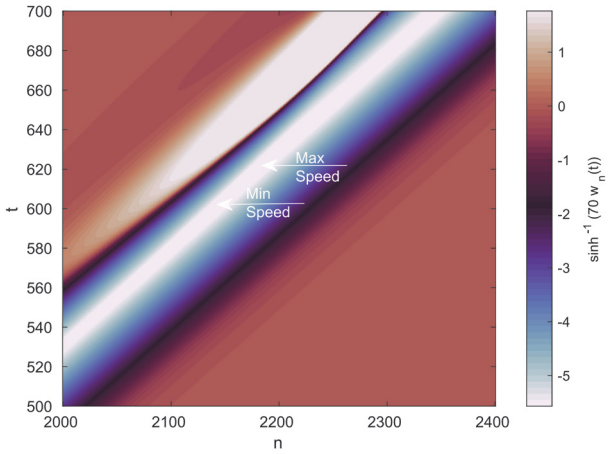

Figure 12: An enlarged view of the space-time plot Fig. 11(a). The arrows mark the points corresponding to the minimal and maximal values of the wave's velocity in Fig. 10(a).

linear interactions may give rise to stability changes. To this end, we considered the model where the nearest neighbors feature an α-FPU interaction, while interactions beyond nearest neighbors are harmonic with exponentially decaying strength, and investigated different parameter regimes. The regime where the strength and rate of decay of the longer-range interactions were such that the energy H of solitary traveling waves was a nonmonotone function of their velocity c (N-region) was observed to yield instability when $H'(c) < 0$, in line with earlier work. A more detailed study was also performed in Z-region of the parameter space where $H(c)$ was not even single-valued. There, it was revealed that instability corresponds to $H'(s) < 0$, where s is a parameter along the energy-velocity curve. In the Appendix we proved that the change in the sign of $H'(s)$ is associated with the increase of the multiplicity of the zero eigenvalue.

A focal point of the present study concerned the dynamics of unstable solutions in the regions where Floquet multipliers μ of the associated spectral stability analysis were found to be $\mu > 1$.

There, it was seen that it is possible to "kick" the unstable waveforms through suitable multiples of the eigenvector associated with the instability to induce them to acquire a higher velocity, or recede to a lower speed. In each of the cases, the velocity modification was accompanied by the concurrent emission of a suitable coherent structure, typically represented by a slower pulse in the speeding-up case and a dispersive shock wave when slowing-down. Such possibilities were explored in both N and Z parameter regions.

Numerous questions arise as possible extensions of the present work towards future study. In particular, it is important to understand on a more general level what fundamental ingredients a physical setting must have in order to induce the kind of competition that leads to $H'(c) < 0$ and the associated instability as is the case herein. An interesting and highly nontrivial extension of the present study in a one-dimensional lattice setting would involve going beyond traveling waves and examining breathers that bear a further internal frequency (in addition to the traveling one). Finally, studies of solitary traveling waves in lattices have been mostly limited to one-dimensional setting, and little is known about existence and stability of such structures in higher dimensions. A systematic investigation of this issue in a suitably chosen model would be a topic of interest in its own right.

Acknowledgements. This work was supported by the U.S. National Science Foundation (DMS-1808956, AV and DMS-1809074, PGK) and by the National Natural Science Foundation of China (NSFC-11801191, HX). We thank R. Pego for useful discussions and J. Cuevas-Maraver for sharing computer codes that were adapted to perform a number of computations presented herein.

Appendix: stability analysis

In this Appendix, we derive the condition for the change in multiplicity of the zero eigenvalue that generalizes the corresponding condition in [17, 18, 30, 31] to the case when the energy of a STW is not necessarily a single-valued function of its velocity. As in [30, 31], we consider a more general Hamiltonian than in [17, 18] that goes beyond nearest-neighbor interactions. However, in [30, 31] the effect of essential spectrum of the linearization operator was neglected in the derivation of the stability criterion and perturbation results. Moreover, the proof was provided for the displacement formulation and assumed localized displacements. Following [17, 18], here we consider the strain formulation more appropriate for the problem at hand and work with weighted spaces that shift the essential spectrum into the left half-plane.

Weighted spaces, skew symmetry and essential spectrum

Consider a Hamiltonian system in the form

$$H = \sum_{n\in\mathbb{Z}} \left(\frac{1}{2} p_n^2 + U_n(w) \right) = \sum_{n\in\mathbb{Z}} H_n(w(t), p(t)), \tag{14}$$

where $p(t) = [p_n(t)]$ is an infinite vector of particle momenta, $w(t) = [w_n(t)]$ is the strain vector, and the potential energy term $U_n(w)$ may include long-range interactions as in (1). The dynamics of the lattice are governed by

$$\frac{d}{dt} r(t) = \mathcal{J} \frac{\partial H}{\partial r}, \quad r(t) = \begin{pmatrix} w(t) \\ p(t) \end{pmatrix}, \quad \mathcal{J} = \begin{pmatrix} 0 & e^{\partial} - I \\ I - e^{-\partial} & 0 \end{pmatrix}. \tag{15}$$

Here $e^{\pm\partial}$ are the shift operators satisfying $\left(e^{\pm\partial} x\right)_i = x_{i\pm1}$, and I is the identity operator.

Remark 1. *The operator $\mathcal{J}$ is invertible on space $\ell^2 \times \ell^2$, but the inverse is not bounded in this space because zero is in the essential spectrum of $\mathcal{J}$. In particular, if $\mathbf{1}$ represents a vector with all elements being 1, then $\mathcal{J}\begin{pmatrix} c_1\mathbf{1} \\ c_2\mathbf{1} \end{pmatrix}$ vanishes for any c_1 and c_2. By using weighted spaces, one can make $\mathcal{J}$ a one-to-one function and change the essential spectrum of $\mathcal{J}$ so that its inverse is bounded. In particular, if $a > 0$ and $\ell^2_{\pm a} = \{u : \sum_{j\in\mathbb{Z}} |u_j|^2 e^{\pm 2aj} < \infty\}$, then the inverse of $\mathcal{J}$ on $\ell^2_a \times \ell^2_a$ is explicitly given by*

$$\mathcal{J}^{-1}_{a,a} = \begin{pmatrix} 0 & -\sum_{k=1}^{\infty} e^{k\partial} \\ -\sum_{k=0}^{\infty} e^{k\partial} & 0 \end{pmatrix} \tag{16}$$

and the inverse of J on $\ell^2_{-a} \times \ell^2_{-a}$ is of the form

$$\mathcal{J}^{-1}_{-a,-a} = \begin{pmatrix} 0 & \sum_{k=0}^{-\infty} e^{k\partial} \\ \sum_{k=-1}^{-\infty} e^{k\partial} & 0 \end{pmatrix}. \tag{17}$$

In particular, $\mathcal{J}^{-1}_{a,a} u = \mathcal{J}^{-1}_{-a,-a} u$ when $u \in (\ell^2_a \cap \ell^2_{-a}) \times (\ell^2_a \cap \ell^2_{-a})$ and

$$\begin{pmatrix} \sum_{k=-\infty}^{\infty} e^{k\partial} & 0 \\ 0 & \sum_{k=-\infty}^{\infty} e^{k\partial} \end{pmatrix} u = 0.$$

Remark 2. *If one considers $\mathcal{J}$ on $\ell^2 \times \ell^2$, then its adjoint is also viewed as an operator on $\ell^2 \times \ell^2$, and in particular $\mathcal{J}^* = -\mathcal{J}$, which implies that J is skew-symmetric. If $\mathcal{J}$ is defined on $\ell^2_a \times \ell^2_a$, then its adjoint $\mathcal{J}^*_{a,a}$ can be viewed as on $\ell^2_{-a} \times \ell^2_{-a}$. Since we can also treat $\mathcal{J}$ as an operator $\mathcal{J}_{-a,-a}$ on $\ell^2_{-a} \times \ell^2_{-a}$, then*

$$\langle u, \mathcal{J}_{a,a} v\rangle_{\ell^2\times\ell^2} + \langle \mathcal{J}_{-a,-a} u, v\rangle_{\ell^2\times\ell^2} = 0$$

where $u \in \ell^2_a \times \ell^2_a$, $v \in \ell^2_{-a} \times \ell^2_{-a}$ and $\langle\cdot,\cdot\rangle_{\ell^2\times\ell^2}$ represents the inner product on $\ell^2 \times \ell^2$. This property can be equivalently written as $\mathcal{J}^*_{a,a} = -\mathcal{J}_{-a,-a}$ and it is another version of the skew-symmetry. Moreover, since $\mathcal{J}^{-1}$ has different inverses on different weighted spaces, it in general does not inherit the skew symmetry from $\mathcal{J}$.

We now assume that (15) has a smooth family of solitary traveling wave solutions which have the form

$$r_{tw}(t;s) = \begin{pmatrix} w_{tw}(t;s) \\ p_{tw}(t;s) \end{pmatrix}, \qquad w_{tw,n}(t;s) = \hat{w}(\xi(s)), \qquad p_{tw,n}(t;s) = \hat{p}(\xi(s)), \tag{18}$$

where $\xi(s) = n - c(s)t$ and $c(s)$ is the velocity of the wave, which is strictly above the sound speed and depends on the parameter s. We assume that s provides a regular parametrization of the energy-velocity curve, so that $c'(s)$ and $H'(s)$ do not vanish simultaneously. This parametrization is not necessarily unique. It is convenient to use rescaled time $\tau = c(s)t$, so that the wave period is rescaled to one. Then we have

$$\frac{dR}{d\tau} = \frac{1}{c(s)} \mathcal{J} \frac{\partial H}{\partial R}, \quad R(\tau) = \begin{pmatrix} W(\tau) \\ P(\tau) \end{pmatrix} = r(t). \tag{19}$$

Linearizing (19) around the solution $R_{tw} = \begin{pmatrix} W_{tw} \\ P_{tw} \end{pmatrix}$ with $R(\tau) = R_{tw}(\tau) + \epsilon S(\tau)$, we find

$$\frac{dS}{d\tau} = \frac{1}{c(s)} \mathcal{J} \frac{\partial^2 H}{\partial R^2}\bigg|_{R=R_{tw}} S(\tau). \tag{20}$$

We consider perturbations in the form $S(\tau) = S_{tw}(\tau) e^{\nu\tau}$, where

$$S_{tw} = \begin{pmatrix} X_{tw} \\ Y_{tw} \end{pmatrix}$$

is a traveling wave with unit velocity; i.e., periodic modulo shift with period 1. This yields the eigenvalue problem

$$\mathcal{L}S_{tw}(\tau) = \nu S_{tw}(\tau) \tag{21}$$

for the linear operator

$$\mathcal{L} := \frac{1}{c(s)}\mathcal{J}\frac{\partial^2 H}{\partial R^2}\bigg|_{R=R_{tw}} - \frac{d}{d\tau} \tag{22}$$

with eigenvalue ν, which is related to the eigenvalue λ used in the main text via $\nu = \lambda/c(s)$ due to the time rescaling. Note also that Floquet multiplier μ is related to ν via $\mu = e^{\nu}$. For the Hamiltonian (1) the eigenvalue problem becomes

$$\begin{aligned} &-\frac{d}{d\tau}\begin{pmatrix} X_{tw,j}(\tau) \\ Y_{tw,j}(\tau) \end{pmatrix} + \frac{1}{c(s)}\begin{pmatrix} Y_{tw,j+1}(\tau) - Y_{tw,j}(\tau) \\ V''(W_{tw,j}(\tau))X_{tw,j}(\tau) - V''(W_{tw,j-1}(\tau))X_{tw,j-1}(\tau) \end{pmatrix} \\ &+\frac{1}{c(s)}\begin{pmatrix} 0 \\ \sum_{m=1}^{\infty}\Lambda(m)\left[\sum_{l=0}^{m-1} X_{tw,j+l}(\tau) - \sum_{l=-m}^{-1} X_{tw,j+l}(\tau)\right] \end{pmatrix} = \nu\begin{pmatrix} X_{tw,j}(\tau) \\ Y_{tw,j}(\tau) \end{pmatrix}. \end{aligned} \tag{23}$$

In order to investigate the case with well-localized perturbations S_{tw} (that belong to spaces like $(\ell^2_a \cap \ell^2_{-a}) \times (\ell^2_a \cap \ell^2_{-a})$), we view $\mathcal{L}$ as an operator densely defined on $D^0_{tw,a,a}([0,1])$ with domain $D^1_{tw,a,a}([0,1])$, where

$$\begin{aligned} D^0_{tw,a,a}([0,1]) := \Bigg\{ Z(\tau) = \begin{pmatrix} X(\tau) \\ Y(\tau) \end{pmatrix}, \tau \in [0,1] \Bigg| Z(1) = \begin{pmatrix} e^{-\partial} & 0 \\ 0 & e^{-\partial} \end{pmatrix} Z(0), \\ \int_0^1 \sum_{j\in\mathbb{Z}} (|X_j(\tau)|^2 e^{2a(j-\tau)} + |Y_j(\tau)|^2 e^{2a(j-\tau)}) d\tau < \infty \Bigg\} \end{aligned}$$

and

$$\begin{aligned} D^1_{tw,a,a}([0,1]) := \Bigg\{ Z(\tau) = \begin{pmatrix} X(\tau) \\ Y(\tau) \end{pmatrix}, \tau \in [0,1] \Bigg| Z(1) = \begin{pmatrix} e^{-\partial} & 0 \\ 0 & e^{-\partial} \end{pmatrix} Z(0), \\ \int_0^1 \sum_{j\in\mathbb{Z}} [(|X_j(\tau)|^2 + |X_j'(\tau)|^2) e^{2a(j-\tau)} + (|Y_j(\tau)|^2 + |Y_j'(\tau)|^2) e^{2a(j-\tau)}] d\tau < \infty \Bigg\}, \end{aligned}$$

with prime denoting the time derivative. Following the steps similar to the discussion about $\mathcal{J}$ on $\ell^2_a \times \ell^2_a$, we can also show that $\mathcal{J}$ has a bounded inverse on $D^0_{tw,a,a}([0,1])$.

We note that when $\mathcal{L}$ is considered on unweighted spaces such as $D^0_{tw,0,0}([0,1])$, zero is usually embedded in the essential spectrum of $\mathcal{L}$. To be specific, consider the Hamiltonian (1). Since R_{tw} tends to zero and $V''(0) = 1$, the limiting operator $\mathcal{L}_\infty$ can be defined as

$$\begin{aligned} \mathcal{L}_\infty\begin{pmatrix} X_{tw,j}(\tau) \\ Y_{tw,j}(\tau) \end{pmatrix} &= -\frac{d}{d\tau}\begin{pmatrix} X_{tw,j}(\tau) \\ Y_{tw,j}(\tau) \end{pmatrix} + \frac{1}{c(s)}\begin{pmatrix} Y_{tw,j+1}(\tau) - Y_{tw,j}(\tau) \\ X_{tw,j}(\tau) - X_{tw,j-1}(\tau) \end{pmatrix} \\ &+\frac{1}{c(s)}\begin{pmatrix} 0 \\ \sum_{m=1}^{\infty}\Lambda(m)\left[\sum_{l=0}^{m-1} X_{tw,j+l}(\tau) - \sum_{l=-m}^{-1} X_{tw,j+l}(\tau)\right] \end{pmatrix} \end{aligned} \tag{24}$$

Substituting

$$\begin{pmatrix} X_{tw,j}(\tau) \\ Y_{tw,j}(\tau) \end{pmatrix} = e^{ik(j-\tau)}\begin{pmatrix} b_1 \\ b_2 \end{pmatrix}$$

into $\nu S_{tw} = \mathcal{L}_\infty S_{tw}$ and using $\Lambda(m) = J(e^\alpha - 1)e^{-\alpha|m|}$, $m = 1, 2, \ldots$, one can compute the essential spectrum (similar to [18]) of $\mathcal{L}$ on $D^0_{tw,0,0}([0,1])$ in the form

$$\left\{\nu = i\left(k \pm \frac{2}{c(s)} \sin\frac{k}{2}\sqrt{1 + \frac{J(e^\alpha + 1)}{2(\cosh\alpha - \cos k)}}\right),\ k \in \mathbb{R}\right\}. \tag{25}$$

Thus in this case the essential spectrum is along the imaginary axis and includes 0. Similarly, the essential spectrum of $\mathcal{L}$ on $D^0_{tw,a,a}([0,1])$ with $a > 0$ is obtained by replacing k by $k + ia$ in the above, which yields

$$\begin{aligned}&\left\{\nu = -a + ik \pm \frac{2i}{c(s)}\left(\cosh\frac{a}{2}\sin\frac{k}{2} + i\cos\frac{k}{2}\sinh\frac{a}{2}\right)\times\right.\\ &\left.\sqrt{1 + \frac{J(e^\alpha + 1)}{2(\cosh\alpha - \cos k\cosh a + i\sin k\sinh a)}},\ k \in \mathbb{R}\right\}.\end{aligned} \tag{26}$$

One can show that for $c(s) > c_{\rm s}$, where we recall that $c_{\rm s}$ is the sound speed defined in (6), the essential spectrum in this case is contained in the left half plane $\mathrm{Re}(\nu) < 0$ (and thus does not include zero) for $0 < a < a_c$, where $a_c > 0$ is the exponential decay rate of R_{tw}. It satisfies

$$\frac{2}{c(s)}\sqrt{1 + \frac{J(1 + e^\alpha)}{2(\cosh\alpha - \cosh a_c)}}\sinh\frac{a_c}{2} - a_c = 0 \tag{27}$$

For $J > 0$, we have $0 < a_c < \alpha$, with a_c tending to zero as $c \to c_{\rm s}$ and to α as $c \to \infty$. At $J = 0$, a_c solves $2\sinh(a_c/2) = a_c c(s)$ [18].

Multiplicity of the zero eigenvalue

We now differentiate (19) with respect to τ to obtain

$$\frac{d^2R}{d\tau^2} = \frac{1}{c(s)}\mathcal{J}\frac{\partial^2 H}{\partial R^2}\frac{dR}{d\tau}. \tag{28}$$

Rearranging (28) and evaluating it at $R = R_{tw}$ then yields $\mathcal{L}(\partial_\tau R_{tw})$=0. Thus $e_0 := \partial_\tau R_{tw}$ is an eigenvector of $\mathcal{L}$ with eigenvalue $\nu = 0$ if $e_0 \in D^0_{tw,a,a}([0,1])$. Multiplying (19) by $c(s)$ and differentiating the result with respect to s, we obtain

$$c'(s)\partial_\tau R + c(s)\partial_s\partial_\tau R = \mathcal{J}\frac{\partial^2 H}{\partial R^2}\partial_s R$$

Evaluating this equation at $R = R_{tw}$, we obtain

$$\mathcal{L}(c(s)\partial_s R_{tw}) = c'(s)e_0, \tag{29}$$

which for $c'(s) \neq 0$ yields

$$\mathcal{L}(e_1) = e_0, \qquad e_1 := \frac{c(s)}{c'(s)}\partial_s R_{tw}.$$

Thus e_1 is a generalized eigenvector of $\mathcal{L}$ for eigenvalue $\nu = 0$ if $e_0, e_1 \in D^0_{tw,a,a}([0,1])$. Here we assume

$$e_0, e_1 \in D^0_{tw,-a,-a}([0,1]) \cap D^0_{tw,a,a}([0,1]), \tag{30}$$

which holds when (positive) a is less than a_c, the exponential decay rate of R_{tw}, which for our problem solves (27). This assumption then implies that the multiplicity of eigenvalue $\nu = 0$ is always no less

than two. To further investigate the multiplicity of the eigenvalue $\nu = 0$, we consider the adjoint of $\mathcal{L}$ as

$$\mathcal{L}^* = \frac{d}{d\tau} - \frac{1}{c(s)} \frac{\partial^2 H}{\partial R^2}\bigg|_{R=R_{tw}} \mathcal{J}, \tag{31}$$

on $D^0_{tw,-a,-a}([0,1])$. Suppose that $\mathcal{L}_{-a,-a}$ has the same form of $\mathcal{L}$, but it is restricted on $D^0_{tw,-a,-a}([0,1])$, the adjoint of $\mathcal{L}$ for $Z \in D^0_{tw,-a,-a}([0,1])$ can then be written as

$$\mathcal{L}^* Z = -\mathcal{J}^{-1}_{-a,-a} \mathcal{L}_{-a,-a} \mathcal{J} Z. \tag{32}$$

Consider the generic case when $c'(s) \neq 0$ and $\ker(\mathcal{L}) = \text{span}\{e_0\}$ and similarly $\ker(\mathcal{L}^*) = \text{span}\{\mathcal{J}^{-1}_{-a,-a} e_0\}$, where we note that $\mathcal{L}^*(\mathcal{J}^{-1}_{-a,-a} e_0) = 0$. From the definition of e_0, it can be examined that

$$\mathcal{J}^{-1}_{a,a} e_0 = \mathcal{J}^{-1}_{-a,-a} e_0. \tag{33}$$

Since $\langle \mathcal{J}^{-1}_{-a,-a} e_0, e_0 \rangle = \langle e_0, \mathcal{J}^{-1}_{a,a} e_0 \rangle$, it follows $\langle \mathcal{J}^{-1}_{-a,-a} e_0, e_0 \rangle = 0$. When $\mathcal{L}$ is defined on $D^1_{tw,a,a}([0,1]) \subset D^0_{tw,a,a}([0,1])$, where $0 < a < a_c$, with a_c defined in (27) for Hamiltonian (1), it is a densely-defined closed operator and the use of weighted spaces makes 0 outside the essential spectra of $\mathcal{L}$ and $\mathcal{L}^*$. As a result, $\mathcal{L}$ has closed range and $e_0 \in (\ker(\mathcal{L}^*))^\perp = \text{rng}(\mathcal{L})$. Hence there exists e_1 such that $\mathcal{L}(e_1) = e_0$. Since the energy of the system is conserved, we have that

$$H(s) = \int_0^1 H|_{R_{tw}(\tau;s)} d\tau.$$

We will use this to show that $H'(s) = 0$ if and only if $\langle \mathcal{J}^{-1}_{-a,-a} e_0, e_1 \rangle = 0$. Indeed,

$$\begin{aligned} 0 = \left\langle e_1, \mathcal{J}^{-1}_{-a,-a} e_0 \right\rangle &= \left\langle \frac{c(s)}{c'(s)} \partial_s R_{tw}, \mathcal{J}^{-1}_{a,a} \partial_\tau R_{tw} \right\rangle = \left\langle c(s) \partial_s R_{tw}, \frac{1}{c(s)} \frac{\partial H}{\partial R}\bigg|_{R=R_{tw}} \right\rangle \frac{1}{c'(s)} \\ &= \frac{1}{c'(s)} \int_0^1 \partial_s R_{tw} \left(\frac{\partial H}{\partial R} \right)\bigg|_{R=R_{tw}} d\tau = \frac{1}{c'(s)} \int_0^1 H'(s)|_{R=R_{tw}(\tau;s)} d\tau = \frac{H'(s)}{c'(s)} \end{aligned} \tag{34}$$

Thus, whenever $H'(s) = 0$, we have that $e_1 \in \text{rng}(\mathcal{L})$, and hence there exists e_2 satisfying $\mathcal{L}(e_2) = e_1$, implying that the algebraic multiplicity of $\nu = 0$ is at least three. Moreover, $\mathcal{L}^*(-\mathcal{J}^{-1}_{-a,-a} e_1) = \mathcal{J}^{-1}_{-a,-a} \mathcal{L} \mathcal{J} \mathcal{J}^{-1}_{-a,-a} e_1 = \mathcal{J}^{-1}_{-a,-a} e_0$ implies that

$$\langle \mathcal{J}^{-1}_{-a,-a} e_0, e_2 \rangle = \langle -\mathcal{L}^* \mathcal{J}^{-1}_{-a,-a} e_1, e_2 \rangle = \langle \mathcal{J}^{-1}_{-a,-a} e_1, \mathcal{L} e_2 \rangle = \langle \mathcal{J}^{-1}_{-a,-a} e_1, e_1 \rangle. \tag{35}$$

Since in general

$$\begin{pmatrix} \sum_{k=-\infty}^{\infty} e^{k\partial} & 0 \\ 0 & \sum_{k=-\infty}^{\infty} e^{k\partial} \end{pmatrix} e_1 \neq 0,$$

we have $\langle \mathcal{J}^{-1}_{-a,-a} e_1, e_1 \rangle \neq 0$, and hence the multiplicity of the eigenvalue $\nu = 0$ is at most three.

The change of multiplicity of $\nu = 0$ from two to three suggests that $s = s_0$ such that $H'(s_0) = 0$ corresponds to a stability threshold. The fact that the multiplicity at the threshold becomes three and not four, as suggested by our numerical computations that show collision of eigenvalue pairs typical for Hamiltonian systems [46], is the consequence of the use of the weighted spaces in the strain formulation that destroys the Hamiltonian structure of the problem. In contrast, in [31], where the Hamiltonian structure was preserved, the eigenvalue zero splits as $\nu \sim \sqrt{c - c_0}$ near the critical speed c_0 in when $H''(c_0) \neq 0$ and $\nu = 0$ has multiplicity four at $c = c_0$. Due to the similarity between $\mathcal{J}$ in our problem and ∂_x in [47], a possible scenario for stability change in the present setting is a resonance pole (a pole

of the analytic continuation of the resolvent) moving across the imaginary axis as s crosses s_0 from the upper sheet of the Riemann surface for the resolvent to the lower sheet and emerging as a real positive eigenvalue during the transition from stability to instability [47]. This implies that although the zero eigenvalue has an odd multiplicity at $s = s_0$ in current space, the multiplicity could be even in a larger space. In fact, our numerical computation of the eigenvalues near s_0 shows that the eigenvalue splitting is in the form $\nu \sim \sqrt{s - s_0}$ (see Fig. 9). That is to say, the Hamiltonian symmetry can be retained under certain circumstances, and we will provide an explanation for that below.

Numerical implementations and Hamiltonian symmetry

It should be noted that the results of the numerical eigenvalue problem very much depend on the choices in its implementation. For instance, if we consider a finite chain in the numerical calculation and discretize the variables in time, then the operators such as $\mathcal{J}$, $\frac{d}{d\tau}$ and $\mathcal{L}$ are represented by matrices $[\mathcal{J}]$, $[\frac{d}{d\tau}]$ and $[\mathcal{L}]$, respectively. In particular, if the matrices for $\mathcal{J}$ and $\frac{d}{d\tau}$ are invertible and skew-symmetric, say,

$$\left[\frac{d}{d\tau}\right] = \begin{pmatrix} D & \\ & D \end{pmatrix}, \quad D = \frac{1}{2\Delta\tau}\begin{pmatrix} 0 & 1 & & & \\ -1 & 0 & 1 & & \\ & \cdots & \cdots & \cdots & \\ & & -1 & 0 & 1 \\ & & & -1 & 0 \end{pmatrix},$$

$$[\mathcal{J}] = \begin{pmatrix} 0 & J_1 \\ -J_1^T & 0 \end{pmatrix}, \quad J_1 = \begin{pmatrix} -1 & 0 & \dots & 0 & 1 & & & & \\ & -1 & 0 & \dots & 0 & 1 & & & \\ & & \cdots & \cdots & \cdots & \cdots & \cdots & & \\ & & & \cdots & \cdots & \cdots & \cdots & \cdots & \\ & & & & -1 & 0 & \dots & 0 & 1 \\ & & & & & -1 & 0 & \dots & 0 \\ & & & & & & -1 & 0 & \dots \\ & & & & & & & \cdots & \cdots \\ & & & & & & & & -1 \end{pmatrix}$$

and

$$[\mathcal{J}^{-1}] = [\mathcal{J}]^{-1} = \begin{pmatrix} 0 & -(J_1^T)^{-1} \\ (J_1)^{-1} & 0 \end{pmatrix},$$

then naturally $[\mathcal{J}^{-1}]$ is also skew-symmetric and the multiplicity of zero eigenvalue for $[\mathcal{L}]$ will be even.

As another example, suppose we consider a finite cyclic chain and choose $[\mathcal{J}]$, $[\frac{d}{d\tau}]$ and $[\mathcal{L}]$ so that their kernels contain $\begin{pmatrix} c_1\mathbf{1} \\ c_2\mathbf{1} \end{pmatrix}$. Since this is a finite chain, if $[\mathcal{L}]e_0 = 0$ and $[\mathcal{L}]e_1 = e_0$, we can choose c_1 and c_2 such that $\tilde{e}_1 = \begin{pmatrix} \tilde{e}_1^{(1)} \\ \tilde{e}_1^{(2)} \end{pmatrix} = e_1 - \begin{pmatrix} c_1\mathbf{1} \\ c_2\mathbf{1} \end{pmatrix}$ satisfies $\sum_{k=-\infty}^{\infty} \tilde{e}_{1,k}^{(1)} = \sum_{k=-\infty}^{\infty} \tilde{e}_{1,k}^{(2)} = 0$. Observe that violation of this condition causes the zero eigenvalue to have odd multiplicity in the above discussion. In this setting, we consider the equivalence classes $\{\tilde{e}\}$ modulo $\begin{pmatrix} c_1\mathbf{1} \\ c_2\mathbf{1} \end{pmatrix}$ with representatives $\tilde{e} = \begin{pmatrix} \tilde{e}^{(1)} \\ \tilde{e}^{(2)} \end{pmatrix}$ satisfying $\sum_{k=-\infty}^{\infty} \tilde{e}_k^{(1)} = \sum_{k=-\infty}^{\infty} \tilde{e}_k^{(2)} = 0$. This way we can make $[\mathcal{J}^{-1}]$ skew-symmetric, and hence the zero eigenvalue of $[\mathcal{L}]$ should have even multiplicity.

These two examples illustrate how Hamiltonian symmetry can be retained in a finite-dimensional implementation. A full charaterization of the eigenvalues near zero in different spaces is beyond the scope of this work and is left for future investigations.

References

[1] E. Fermi, J. Pasta, and S. Ulam. Studies of nonlinear problems. Technical Report LA-1940, Los Alamos Scientific Laboratory, 1955.

[2] N. J. Zabusky and M. D. Kruskal. Interaction of solitons in a collisionless plasma and the recurrence of initial states. *Phys. Rev. Lett.*, 15(6):240–243, 1965.

[3] R. Hirota and K. Suzuki. Theoretical and experimental studies of lattice solitons in nonlinear lumped networks. *Proc. IEEE*, 61(10):1483–1491, 1973.

[4] T. Kofane, B. Michaux, and M. Remoissenet. Theoretical and experimental studies of diatomic lattice solitons using an electrical transmission line. *J. Phys. C*, 21(8):1395, 1988.

[5] C. Coste, E. Falcon, and S. Fauve. Solitary waves in a chain of beads under Hertz contact. *Phys. Rev. E*, 56:6104–6117, 1997.

[6] V. Nesterenko. *Dynamics of heterogeneous materials*. Springer, 2001.

[7] E. Kim, R. Chaunsali, H. Xu, J. Jaworski, J. Yang, P. G. Kevrekidis, and A. F. Vakakis. Nonlinear low-to-high-frequency energy cascades in diatomic granular crystals. *Phys. Rev. E*, 92(6):062201, 2015.

[8] B. Deng, Y. Zhang, Q. He, V. Tournat, P. Wang, and K. Bertoldi. Propagation of elastic solitons in chains of pre-deformed beams. *New J. Phys.*, 21(7):073008, 2019.

[9] H. Yasuda, Y. Miyazawa, E. G. Charalampidis, C. Chong, P. G. Kevrekidis, and J. Yang. Origami-based impact mitigation via rarefaction solitary wave creation. *Sci. Adv.*, 5(5):eaau2835, 2019.

[10] S. Shrivastava, K. H. Kang, and M. F. Schneider. Solitary shock waves and adiabatic phase transition in lipid interfaces and nerves. *Phys. Rev. E*, 91(1):012715, 2015.

[11] M. Toda. *Theory of nonlinear lattices*. Springer, Berlin, 1981.

[12] G. Friesecke and J. A. D. Wattis. Existence theorem for solitary waves on lattices. *Communications in Mathematical Physics*, 161(2):391–418, 1994.

[13] D. Smets and M. Willem. Solitary waves with prescribed speed on infinite lattices. *Journal of Functional Analysis*, 149(1):266, 1997.

[14] A. Pankov and V. M. Rothos. Traveling waves in Fermi-Pasta-Ulam lattices with saturable nonlinearities. *Discr. Cont. Dyn. Syst. A*, 30(3):835–849, 2011.

[15] A. Stefanov and P. Kevrekidis. On the existence of solitary traveling waves for generalized hertzian chains. *J. of Non. Sci.*, 22(3):327–349, 2012.

[16] G. Friesecke and R. L. Pego. Solitary waves on Fermi-Pasta-Ulam lattices: I. Qualitative properties, renormalization and continuum limit. *Nonlinearity*, 12:1601–1626, 1999.

[17] G. Friesecke and R. L. Pego. Solitary waves on Fermi-Pasta-Ulam lattices: II. Linear implies nonlinear stability. *Nonlinearity*, 15(4):1343–1359, 2002.

[18] G. Friesecke and R. L. Pego. Solitary waves on Fermi-Pasta-Ulam lattices: III. Howland-type Floquet theory. *Nonlinearity*, 17:202–207, 2004.

[19] G. Friesecke and R. L. Pego. Solitary waves on Fermi-Pasta-Ulam lattices: IV. Proof of stability at low energy. *Nonlinearity*, 17(1):229–251, 2004.

[20] G. Iooss. Travelling waves in the Fermi-Pasta-Ulam lattice. *Nonlinearity*, 13(3):849, 2000.

[21] E. McMillan. Multiscale correction to solitary wave solutions on FPU lattices. *Nonlinearity*, 15(5):1685–1697, 2002.

[22] A. Hoffman and C. Wayne. A simple proof of the stability of solitary waves in the Fermi-Pasta-Ulam model near the KdV limit. In *Infinite dimensional dynamical systems*, pages 185–192. Springer, 2013.

[23] G. Friesecke and K. Matthies. Atomic-scale localization of high-energy solitary waves on lattices. *Physica D*, 171:211–220, 2002.

[24] M. Herrmann and K. Matthies. Asymptotic formulas for solitary waves in the high-energy limit of FPU-type chains. *Nonlin.*, 28(8):2767, 2015.

[25] M. Herrmann and K. Matthies. Stability of high-energy solitary waves in Fermi-Pasta-Ulam-Tsingou chains. *Trans. of the AMS*, 372(5):3425–3486, 2019.

[26] J. B. A. Sonkeng, F. II Ndzana, S. Abdoulkary, and A. Mohamadou. Modulational instabilities and chaotic-like behaviors in repulsive lattices. *Eur. Phys. J. Plus*, 136(2):1–11, 2021.

[27] A. Mehrem, N. Jimenez, L. J. Salmerón-Contreras, X. García-Andrés, L. M. García-Raffi, R. Picó, and V. J. Sánchez-Morcillo. Nonlinear dispersive waves in repulsive lattices. *Phys. Rev. E*, 96(1):012208, 2017.

[28] T. Mizumachi and R. L. Pego. Asymptotic stability of Toda lattice solitons. *Nonlin.*, 21(9):2099, 2008.

[29] G. N. Benes, A. Hoffman, and C. E. Wayne. Asymptotic stability of the Toda m-soliton. *J. Math. Anal. Appl.*, 386(1):445–460, 2012.

[30] J. Cuevas-Maraver, P. Kevrekidis, A. Vainchtein, and H. Xu. Unifying perspective: Hamiltonian lattice traveling waves as discrete breathers and energy criteria for their stability. *Phys. Rev. E*, 96:032214, 2017.

[31] H. Xu, J. Cuevas-Maraver, P. G. Kevrekidis, and A. Vainchtein. An energy-based stability criterion for solitary travelling waves in Hamiltonian lattices. *Phil. Trans. R. Soc. A*, 376(2117):20170192, 2018.

[32] P. G. Kevrekidis, J. Cuevas-Maraver, and D. E. Pelinovsky. Energy criterion for the spectral stability of discrete breathers. *Phys. Rev. Lett.*, 117:094101, Aug 2016.

[33] L. Truskinovsky and A. Vainchtein. Solitary waves in a nonintegrable Fermi-Pasta-Ulam chain. *Phys. Rev. E*, 90(4):042903, 2014.

[34] L. Truskinovsky and A. Vainchtein. Strictly supersonic solitary waves in lattices with second-neighbor interactions. *Phys. D*, 389:24–50, 2019.

[35] S. Katz and S. Givli. Solitary waves in a bistable lattice. *Extr. Mech. Lett.*, 22:106–111, 2018.

[36] S. Katz and S. Givli. Solitary waves in a nonintegrable chain with double-well potentials. *Phys. Rev. E*, 100(3):032209, 2019.

[37] A. Neuper, Y. Gaididei, N. Flytzanis, and F. Mertens. Solitons in atomic chains with long-range interactions. *Phys. Lett. A*, 190(2):165–171, 1994.

[38] Y. Gaididei, N. Flytzanis, A. Neuper, and F. G. Mertens. Effect of nonlocal interactions on soliton dynamics in anharmonic lattices. *Phys. Rev. Lett.*, 75(11):2240–2243, 1995.

[39] Y. Gaididei, N. Flytzanis, A. Neuper, and F. G. Mertens. Effect of non-local interactions on soliton dynamics in anharmonic chains: Scale competition. *Physica D*, 107(1):83–111, 1997.

[40] S. F. Mingaleev, Y. B. Gaididei, and F. G. Mertens. Solitons in anharmonic chains with ultra-long-range interatomic interactions. *Phys. Rev. E*, 61(2):R1044–1047, 2000.

[41] G. A. Baker Jr. One-dimensional order-disorder model which approaches a second-order phase transition. *Phys. Rev.*, 122(5):1477–1484, 1961.

[42] M. Kac and E. Helfand. Study of several lattice systems with long-range forces. *J. Math. Phys.*, 4(8):1078–1088, 1961.

[43] K. S. Viswanathan and D. H. Mayer. Statistical mechanics of one-dimensional ising and potts models with exponential interactions. *Phys. A*, 89(1):97–112, 1977.

[44] S. K. Sarker and J. A. Krumhansl. Effect of solitons on the thermodynamic properties of a system with long-range interactions. *Phys. Rev. B*, 23(5):2374, 1981.

[45] H. B. Keller. *Lectures on Numerical Methods in Bifurcation Problems.* Springer-Verlag, New York, 1986.

[46] V. I. Arnold. *Mathematical methods of classical mechanics.* Springer-Verlag, New York, 1978.

[47] R. L. Pego and M. I. Weinstein. Eigenvalues, and instabilities of solitary waves. *Philosophical Transactions of the Royal Society of London. Series A: Physical and Engineering Sciences*, 340(1656):47–94, 1992.